

Electronic Transitions in Conformationally Controlled Peralkylated Hexasilanes

Yuki Kanazawa,^[a, b] Hayato Tsuji,^{*[c, d]} Masahiro Ehara,^{*[a, b, e]} Ryoichi Fukuda,^[e]
Deborah L. Casher,^[f] Kohei Tamao,^[c, g] Hiroshi Nakatsuji,^[h] and Josef Michl^{*[f, i]}

The photophysical properties of oligosilanes show unique conformational dependence due to σ -electron delocalization. The excited states of the SAS, AAS, and AEA conformations of peralkylated *n*-hexasilanes, in which the SiSiSiSi dihedral angles are controlled into a *syn* (S), *anti* (A), or *eclipsed* (E) conformation, were investigated by using UV absorption, magnetic circular dichroism (MCD), and linear dichroism spectroscopy. Simultaneous Gaussian fitting of all three spectra identified a minimal set of transitions and the wavenumbers, oscillator strengths, and MCD *B* terms in all three compounds. The re-

sults compare well with those obtained by using the symmetry-adapted-cluster configuration interaction method and almost as well with those obtained by time-dependent density functional theory with the PBE0 functional. The conformational dependence of the transition energies and other properties of free-chain permethylated *n*-hexasilane, *n*-Si₆Me₁₄, was also examined as a function of dihedral angles, and the striking effects found were attributed to avoided crossings between configurations of $\sigma\sigma^*$ and $\sigma\pi^*$ character.

1. Introduction

Photophysical properties that reflect the delocalization of σ electrons, more complicated and less well understood than the delocalization of π electrons, have received much attention in the context of understanding the electronic properties of catenates of heavier main group elements, such as silicon and phosphorus. σ -Delocalized systems generally show high conformational flexibility, and this could, in principle, be used to control their various optical properties by molecular design. However, this feature has so far not been fully understood or utilized.

The characteristic photophysical and electronic properties of polysilanes and oligosilanes, representative models of σ -delocalized systems with a singly bonded chain carrying lateral

substituents, have been extensively studied (e.g. UV absorption,^[1–9] luminescence,^[5–8,10] nonlinear polarizability,^[11,12] and photoconductivity^[13]) and reviewed.^[14–21] A complete understanding of σ delocalization in simple terms is still far away, due to its strong conformational dependence, as exemplified by the thermochromism^[22–26] of oligosilanes.^[27] Flexible unconstrained permethylated polysilane chains favor three SiSiSiSi dihedral angles, *transoid* (165°), *gauche* (55°), and *ortho* (90°).^[21,28–30] Among these conformations, the thermodynamically most stable *transoid* form predominates at low temperatures^[31] and typically shows an intense long-wavelength absorption band.^[32,33]

[a] Y. Kanazawa, Prof. M. Ehara
SOKENDAI
The Graduate University for Advanced Studies
Nishigonaka, Myodaiji, Okazaki 444–8585 (Japan)
E-mail: ehara@ims.ac.jp

[b] Y. Kanazawa, Prof. M. Ehara
Institute for Molecular Science
and Research Center for Computational Science
Nishigonaka, Myodaiji, Okazaki 444–8585 (Japan)

[c] Prof. H. Tsuji, Prof. K. Tamao
International Research Center for Elements Science (IRCELS)
Institute for Chemical Research
Kyoto University, Uji, Kyoto 611-0011 (Japan)
E-mail: tsujiha@kanagawa-u.ac.jp

[d] Prof. H. Tsuji
Present address: Department of Chemistry
Faculty of Science, Kanagawa University
2946 Tsuchiya, Hiratsuka, Kanagawa 259–1293 (Japan)

[e] Prof. M. Ehara, Prof. R. Fukuda
Elements Strategy Initiative for Catalysts and Batteries (ESICB)
Kyoto University, Kyoto 615–8520 (Japan)

[f] Dr. D. L. Casher, Prof. J. Michl
Department of Chemistry and Biochemistry
University of Colorado at Boulder
Boulder, Colorado 80309-0215 (USA)
E-mail: michl@eefus.colorado.edu

[g] Prof. K. Tamao
Present address: RIKEN, 2-1 Hirosawa
Saitama 351-0198 (Japan)

[h] Prof. H. Nakatsuji
Quantum Chemistry Research Institute
Goryo Oohara 1–36, Nishikyo-ku, Kyoto 615–8245 (Japan)

[i] Prof. J. Michl
Institute of Organic Chemistry and Biochemistry
Academy of Sciences of the Czech Republic
Flemingovo nám. 2, 16610 Prague (Czech Republic)

Supporting Information for this article can be found under: <http://dx.doi.org/10.1002/cphc.201600633>.

Extensive efforts have been made to clarify the conformational effects on the photophysical properties of oligosilanes for various Si–Si chain lengths. The theoretical understanding of *n*-tetrasilanes, the shortest chains that exhibit conformational isomerism, is now well advanced. Computational studies have been published for the ladder C and H models,^[33–37] including conformational analysis,^[28,29,38–42] for the excited states of the *n*-tetrasilanes Si₄H₁₀^[43–45] and *n*-Si₄Me₁₀^[9,34,46–48] and for longer chains.^[33] Experimental studies have dealt with matrix isolation of *n*-Si₄Me₁₀ conformers,^[46,49] conformational control by cyclic carbosilanes,^[6,8,49–52] bicyclic disilanes,^[32,52–56] bicyclic trisilanes,^[57,58] and bulky lateral substituents,^[59] hypervalent silicons,^[60–63] helicity introduction by chiral terminal^[64–66] or lateral^[67,68] substituents; and inclusion into cyclodextrin and other hosts.^[69–74]

Joint theoretical and experimental studies of model tetrasilanes of C₂ symmetry have assigned their excited states to either an A or B irreducible representation. Transitions from the ground state to the A state are usually weak, whereas transitions to at least the lowest and sometimes several B states are often strong. At highly twisted conformations (*cisoid*, small SiSiSiSi dihedral angle), the first transition is to a state with mostly $\sigma\pi^*$ character and the lowest $\sigma\sigma^*$ transition is much higher. At dihedral angles approaching 180° (*anti*), the strong $\sigma\sigma^*$ transition lies below the weak first $\sigma\pi^*$ transition, and this results in an avoided crossing at intermediate dihedral angles. At all dihedral angles, the lowest $\sigma\sigma^*$ component endows a transition with significant oscillator strength, whereas the $\sigma\pi^*$ components hardly contribute to the intensity at all. These general trends were observed in the UV, MCD (magnetic circular dichroism), and LD (linear dichroism) spectra and in the calculated properties of conformationally controlled peralkylated tetrasilanes.^[9,35]

Presently, we turn to Si backbone conformational effects in longer Si chains, which have only been studied in detail theoretically for some model systems^[33] and experimentally in the case of peralkylated *n*-hexasilanes.^[10,21,53,59] So far, conformationally controlled *n*-hexasilanes with lateral bulky substituents (shown in Scheme 1), in which three SiSiSiSi dihedral angles are present, have been synthesized and their UV spectra have been reported.^[21,53] However, detailed analysis of these spectra has not been performed. In particular, the longer chain should reveal richer effects of σ delocalization on electronic excitation, as the combination of three variable dihedral angles may pro-

vide many opportunities to affect σ delocalization in different ways.

We report the UV, MCD, and LD_r (reduced linear dichroism) spectra of conformationally controlled peralkylated hexasilanes 1–3 (Scheme 1). These three compounds contain *syn* (S), *anti* (A), and *eclipsed* (E) SiSiSiSi dihedral angles and shall be referred to as the SAS, AAS, and AEA conformations. As is common for saturated chains, the spectra consist of broad fairly featureless bands, and this makes the recognition of individual electronic transitions difficult. However, we find that simultaneous Gaussian fitting of the three types of spectra is very helpful and permits a detailed analysis.

The observed transitions are interpreted in terms of calculations by using the symmetry-adapted configuration interaction (SAC-CI) method^[75,76] and time-dependent density functional theory (TD-DFT) with the PBE0 functional.^[77] The spectral changes in free-chain permethylated hexasilane *n*-Si₆Me₁₄ (4) are also computed as a function of the backbone dihedral angles. The results represent the first detailed theoretical interpretation of the excited states of hexasilanes as a function of dihedral angles.

Experimental Section and Calculations

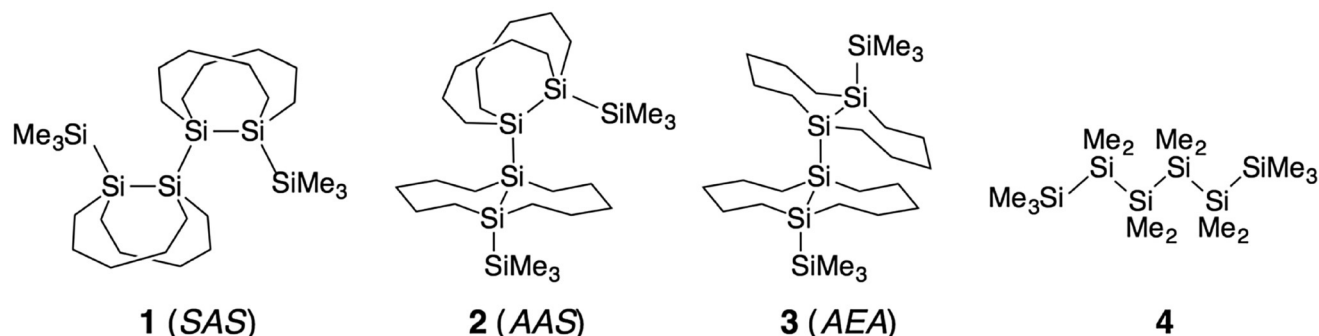
Materials

All hexasilanes were prepared by methods described previously^[53] and were purified thoroughly by recrystallization. 3-Methylpentane was purified by passing through a column of silver nitrate on alumina.^[78]

Spectral Measurements

UV Absorption

UV absorption spectra were recorded with an OLIS RSM 1000 spectrometer with a resolution of 0.5 nm. The spectrometer was calibrated against a holmium oxide filter. About 10^{–5} M sample solutions in 3-methylpentane (3-MP) in a 1 cm square quartz cell were measured at room temperature, and the spectra were converted with Spectracalc into plots of absorptivity ϵ (M^{–1} cm^{–1}) against wavenumber (cm^{–1}). For measurements in a 3-MP glass at 77 K, a solution in a 1 cm wide × 0.3 cm thick quartz cell equipped with a stopcock was immersed in liquid nitrogen in a quartz Dewar with Suprasil windows for at least 5 min before the spectrum was recorded. *D* terms were calculated according to Equation (1) in units of D², where D stands for Debye.^[79]



Scheme 1. Structures of conformationally controlled peralkylated *n*-hexasilanes 1–3 and free permethylated *n*-hexasilane 4.

$$D_i = 9.188 \times 10^{-3} \int_i \frac{\varepsilon}{\tilde{\nu}} d\tilde{\nu} \quad (1)$$

and oscillator strengths f were calculated from Equation (2):

$$f_i = 4.319 \times 10^{-9} \int_i \varepsilon(\tilde{\nu}) d\tilde{\nu} \quad (2)$$

Magnetic Circular Dichroism Spectra

The sample solution ($\approx 10^{-5}$ M in 3-MP) was placed in a 1 cm thick cylindrical cell in the presence of a magnetic field parallel to the light propagation direction. The spectra were recorded with a JASCO J-500C spectrometer equipped with a JASCO electromagnet (1.504 T) with a resolution of 0.5 nm by scanning at 5 nm min⁻¹ with a 4 s response time, and 100–300 scans were averaged to improve the signal/noise ratio. The direction and strength of the magnetic field were calibrated with an aqueous solution of CoSO₄·7H₂O.^[80] The spectra were converted by using Spectralcalc into plots of molar magnetic ellipticity $[\Theta]_M$ (deg m⁻¹ cm⁻¹ G⁻¹) against wavenumber (cm⁻¹). MCD B terms were calculated in units of $D^2 \beta_e$ cm⁻¹ according to Equation (3) for which β_e is the Bohr magneton. Given that the molecular symmetry is low and excludes state degeneracies, the A and C terms are zero for all hexasilanes used:

$$B_i + C_i/kT = -33.53^{-1} \int_i \frac{[\Theta]_M}{\tilde{\nu}} d\tilde{\nu} \quad (3)$$

Linear Dichroism Spectra^[81]

Commercial low-density polyethylene sheets were washed in spectral-grade chloroform for 1 h to remove additives and were cut into roughly 2×2 cm pieces. The small sheets were soaked in a chloroform solution of a hexasilane, washed with methanol to remove any small crystals on the surface, dried overnight, and stretched about 400%.

The spectra were measured with the LD mode of a JASCO J-500C spectrometer. The sample sheet was placed immediately in front of the photomultiplier tube to minimize the effects of light scattering. All spectra were recorded with a resolution of 0.5 nm and were converted into plots of ΔOD against wavenumbers $\tilde{\nu}$ by using Spectralcalc. To obtain the shape of reduced linear dichroism, $LD_r = \Delta OD/OD$ (on an indeterminate vertical scale), the isotropic optical density (OD) was approximated by OD measured at an arbitrary concentration in 3-MP. The LD_r values at the onset of absorption were distorted by the small difference between the OD measured in 3-MP and in polyethylene and were ignored.

Simultaneous Fitting of Room-Temperature Absorption, MCD, and LD_r Spectra

The fitting to a set of Gaussian-shaped peaks to obtain the $\tilde{\nu}$, B , D , and f values was performed by using the Origin program. The results are given in Table 1 and are displayed in Figures S1–S3 (Supporting Information). The position (wavenumber $\tilde{\nu}$), height, and width (full-width-at-half-maximum, FWHM) of each Gaussian were adjustable parameters. The starting points for the fitting were preliminary values obtained by guessing the start and the end of the

bands due to individual transitions from spectral shapes. The number of Gaussians used was the minimum needed for a visually satisfactory fit to all three types of spectra (Figures S1–S3). Although it could be only approximately correct, it was assumed that band positions $\tilde{\nu}$ and widths FWHM were the same in the UV absorption, MCD, and LD spectra. It was further assumed that each absorption band i was purely polarized along some unknown direction in the molecular frame, the average orientation of which in the polyethylene film was characterized by an average value $\langle \cos^2 \theta_i \rangle = K_i$, in which θ_i is the angle between the transition moment and the uniaxial stretching direction Z . Each band would therefore in itself have a constant LD_r value given by $G_i = (3K_i - 1)/2$ (shown on an arbitrary vertical scale by horizontal double lines in Figures S1b–S3b). The observed LD_r curve is a superposition of contributions from all bands, given by Equation (4):

$$LD_r = \frac{\sum_i A_i (3K_i - 1)}{2 \sum_i A_i} \quad (4)$$

in which A_i is the absorbance due to the i -th transition.

The bands associated with individual transitions are not necessarily Gaussian shaped, and more than one Gaussian could correspond to a single transition in the fit. It was assumed that in such a case the ratios of the relative heights and the ratios of the relative widths within the set of Gaussians would be roughly similar in the UV absorption and MCD spectra (similar spectral shapes), and the G_i values associated with the Gaussians would be similar as well (the same polarization).

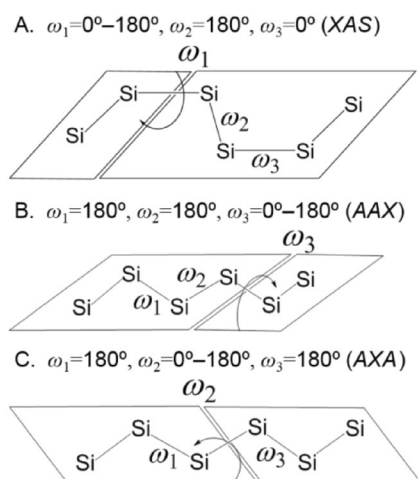
Fitting of Low-Temperature Absorption Spectra

Guided by the results of the simultaneous fitting of three room-temperature spectra, we finally also fitted the somewhat better resolved UV absorption spectra taken at 77 K, and the results are shown in Figure S4.

Computational Details

The conformational effects of the linear hexasilane backbone chain on the absorption energy for peralkylated n -hexasilanes **1–3** and permethylated n -hexasilane **4**, n -Si₆Me₁₄, (Scheme 1) were examined. Ground-state geometry optimizations were performed by the B3LYP^[82]/6-311G(d)^[83] method. Initial geometries for optimization were taken from X-ray crystal structures published previously (Figure S5).^[53] The X-ray crystal structure of **1** contains two distinct conformations with terminal dihedral angles $\omega = 13$ and 30° . For **3**, the positions of the carbon atoms are unclear, and geometry optimization resulted in four different stable conformations. Thus, two C_i conformations were obtained for **1** (SAS), one C_i configuration for **2** (AAS), and two C_i and two C_i configurations for **3** (AEA). All the coordinates were optimized without constraints, and the structures were confirmed to be local minima by vibrational analysis. In **4**, two dihedral angles were fixed in a *syn* ($\omega = 0^\circ$) or *anti* ($\omega = 180^\circ$) conformation and one dihedral angle was varied from 0 to 180° in steps of 30° , as shown in Scheme 2: A) XAS ($\omega_1 = 0-180^\circ$, $\omega_2 = 180^\circ$, $\omega_3 = 0^\circ$), B) AAX ($\omega_1 = 180^\circ$, $\omega_2 = 180^\circ$, $\omega_3 = 0-180^\circ$), and C) AXA ($\omega_1 = 180^\circ$, $\omega_2 = 0-180^\circ$, $\omega_3 = 180^\circ$). All other coordinates were optimized.

Electronic transitions in **1–3** were obtained from SAC-CI and TD-PBE0 calculations. These calculations were done for all the above-



Scheme 2. Conformational changes examined for n -Si₆Me₁₄.

mentioned conformations of the local minima. It is well recognized that TD-PBE0 provides satisfactory results for valence excited states of π -conjugated systems.^[84–87] Therefore, in this work, TD-PBE0 was adopted for the excited states of σ -delocalized systems **1–4** by using the 6-311G(d) basis set. SAC-Cl calculations^[88,89] were performed for vertical transitions of peralkylated n -hexasilanes **1–3**. The perturbation selection of linear operators was employed with LevelThree accuracy; the energy thresholds were $\lambda_g = 1 \times 10^{-6}$ and $\lambda_e = 1 \times 10^{-7}$.^[90] The direct algorithm,^[91] computing all nonlinear terms, was adopted. The basis sets were McLean and Chandler valence triple ζ [6s5p]^[92] with double polarization functions ($\zeta_d = 0.424, 0.118$)^[93] for Si atoms and Huzinaga–Dunning D95v [3s2p/2s]^[93] for C and H atoms. The SAC-Cl dimensions were 600 000–800 000 after the perturbation selection. Recently, benchmark SAC-Cl and TD-PBE0 calculations were performed not only for energy^[86,87,94] but also for charge-transfer properties.^[95,96] All calculations were performed with the developmental version of the Gaussian09 suite of programs^[97] that included a parallelized code for SAC-Cl.

The σ and π character of the frontier molecular orbitals (MOs) of compounds **1–3** relevant to the electronic transitions was determined from natural hybrid orbitals (NHOs) by using a previously described method,^[33] slightly modified to treat the terminal Si atoms in the same fashion as the internal ones. The sets of orthogonal NHOs were calculated by using Gaussian NBO version 3.1.^[98]

2. Results

2.1. UV, MCD, LD, and LD_r Spectra of Conformationally Controlled Peralkylated n -Hexasilanes **1–3**

The UV absorption, MCD, LD, and LD_r spectra of conformationally controlled peralkylated n -hexasilanes **1–3** are displayed in Figure 1. For hexasilane **1** (SAS, red line), the overall Gaussian fits and the individual Gaussian contributions are also shown (for full details, see Figures S1–S4). The numerical data for transition wave numbers $\tilde{\nu}$, oscillator strengths f , and MCD B terms that resulted from simultaneous fitting of the UV, MCD, and LD_r spectra with five (for **1** and **2**) or six (for **3**) Gaussian functions are compiled in Table 1 along with the theoretical results for the SAS-2, AAS, and AEA-3 conformations; results for the

other conformations are provided in the Supporting Information (Tables S5–S8).

The room-temperature UV absorption spectra of **1–3** in 3-MP are shown in Figure 1A. The UV spectra observed at 77 K are shown in Figure 1B. Their absorption bands are sharper and make otherwise hidden transitions more evident. For instance, the faint shoulder at about 42 000 cm⁻¹ in the room-temperature spectrum of AAS-hexasilane **2** becomes quite distinct at low temperature.

The MCD spectra of **1–3** are shown in Figure 1C. They were very helpful for the initial detection of transitions hidden in the UV absorption spectra. Thus, in the low-energy region, SAS hexasilane **1** shows two clear signals instead of a single one in the absorption spectrum: a weak negative band at 41 100 cm⁻¹ that is not detectable in the absorption spectrum and a positive one at 41 900 cm⁻¹ that fits the first UV absorption band. In AAS hexasilane **2**, the strong UV absorption band at 39 000 cm⁻¹ appears only relatively weakly in the MCD spectrum, which underscores the importance of additional transitions at higher energies. Similarly as in SAS, the negative–positive–negative MCD pattern observed in AEA hexasilane **3** at about 39 000, 42 000, and 48 000 cm⁻¹ reveals transitions that would be at best only suspected in absorption.

The LD (ΔOD) and reduced LD (LD_r, $\Delta OD/OD$) spectra of **1–3** are shown in Figure 1D. The LD_r spectra also point out the presence of transitions hidden in the ordinary absorption spectra. For example, the presence of a transition at energies lower than the first absorption band of **1**, the distinct nature of the faint absorption shoulder in **2** near 42 000 cm⁻¹, and the presence of a transition just above 41 000 cm⁻¹ in **3** are clearly indicated.

Although one might attempt to identify the individual transitions in **1–3** on the basis of such qualitative observations, the simultaneous fitting with Gaussians that we finally used (Table 1) is clearly less subjective and more reliable.

2.2. Calculated Ground-State Geometries of Peralkylated n -Hexasilanes **1–3**

The calculated ground-state geometrical parameters of peralkylated n -hexasilanes **1–3**, SAS, AAS and AEA, optimized by B3LYP/6-311G(d), are summarized in Tables S2–S4. As noted above, starting an unconstrained optimization at the two distinct conformations present in the crystal of **1** (SAS) in a 1:1 ratio yielded two stable C_i structures for the molecule of **1**, close in energy. The three calculated SiSiSiSi dihedral angles were $\omega = 21, 180,$ and -21° and $\omega = 13, 180,$ and -13° (Table S2). Another local minimum structure of C_2 symmetry was also obtained. The two C_i conformations are close in energy with a relative energy of 1.1 kcal mol⁻¹, whereas the C_2 conformation is located at 2.6 kcal mol⁻¹ above. The valence angles cover the $\theta = 116$ – 122° range and the five Si–Si bond lengths are in the $r(\text{Si–Si}) = 2.377$ – 2.407 Å range with a weak bond alternation (less than 0.02 Å). This shows that the geometrical strain due to lateral carbon bridges is relatively small and that the n -hexasilane backbone is close to that in free n -Si₆Me₁₄ with the same dihedral angles. The geometrical param-

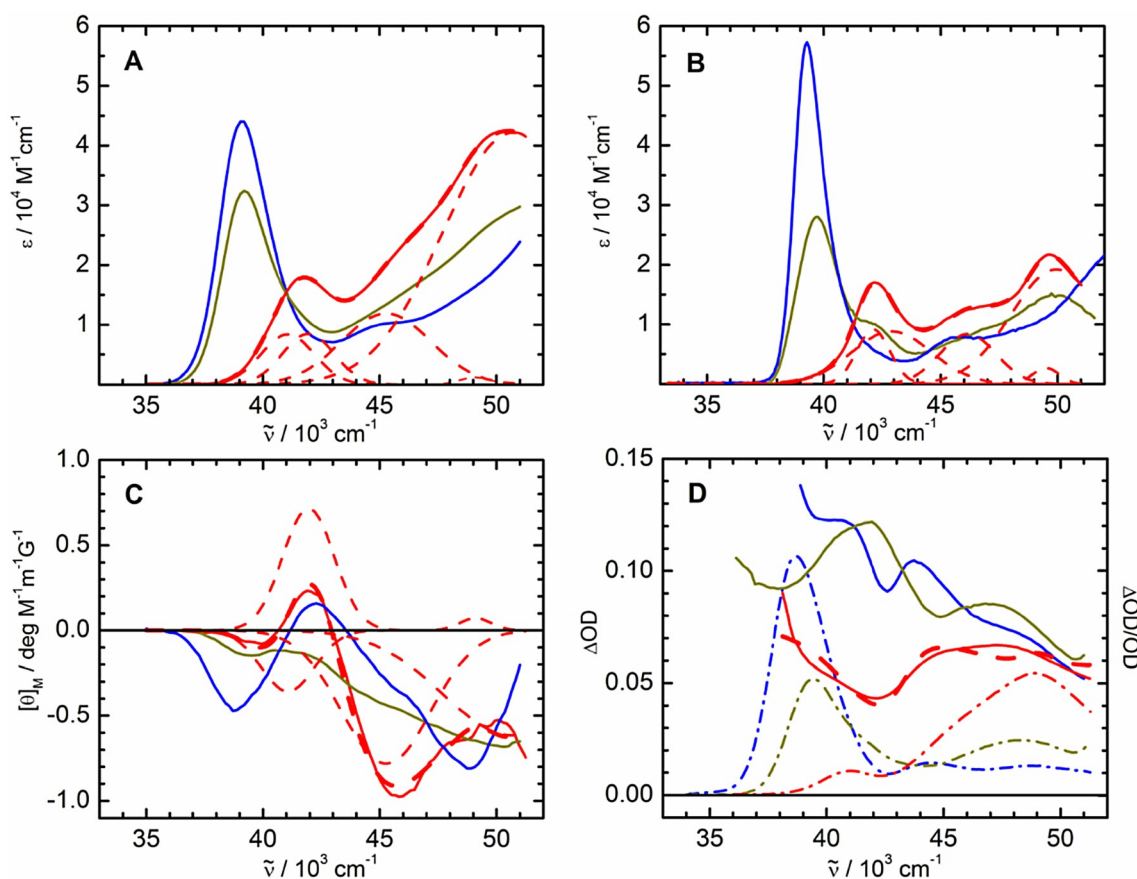


Figure 1. Spectra of **1** (SAS; red), **2** (AAS; dark yellow), and **3** (AEA; blue) in 3-MP: UV absorption at A) room temperature and B) 77 K (corrected for solvent contraction by a factor of 0.784), C) MCD, and D) LD (dash-dot line) and LD, (full line). The red lines show the Gaussian fit for **1** (long dashes) and the individual Gaussian contributions (short dashes).

eters of **2** (AAS) and **3** (AEA) also exhibit a similar trend. Starting from the crystal structure, the dihedral angles in **2** were calculated as $\omega = 180, 178,$ and 14° . There are four possible conformations in the X-ray crystal structure of **3**. Geometry optimizations gave two conformations of C_1 and two of C_2 symmetry with relative energies within $1.0 \text{ kcal mol}^{-1}$. The terminal dihedral angles, ω_1 and ω_3 , range from 167 to 174° , whereas ω_2 ranges from 108 to 130° . The valence angles are in the $\theta = 114\text{--}120^\circ$ range.

2.3. Calculated Electronic Transitions in Peralkylated n -Hexasilanes 1–3

Vertical transitions were calculated at all ground-state optimized structures. The calculated transition energies, oscillator strengths, and description of the nature of the excitations are summarized in Table 1. The SAC-CI and TD-PBE0 calculations gave similar spectral shapes and structures, and the SAC-CI transition wavenumbers were mostly slightly lower and the TD-PBE0 values higher than those observed. The absorption spectra of **1–3** computed by SAC-CI and TD-PBE0 are compared in Figure 2, for which the transitions are convoluted with a Gaussian with a FWHM of 1500 cm^{-1} . MOs related to the transitions are displayed in Figure S6. On the basis of a comparison of the experimental and theoretical spectra, we

summarize the results for the C_1 (SAS-2, $\omega_1 = 13^\circ$) and C_2 (AEA-3) structures for compounds **1** and **3**, respectively, in Table 1. The computational results for the excited states for all the other conformations are compiled in the Supporting Information (Tables S5–S8). The reasons for the selection of the SAS-2 conformer for **1** are discussed below. The calculated absorption spectra of four nearly degenerate conformations of **3** are similar, and AEA-3 was selected because of its higher symmetry, useful for spectral assignments. All MOs that serve as starting orbitals of low-energy excitations are of essentially pure σ character, whereas the terminating orbitals can be predominantly σ^* or π^* in nature, or in a few cases, strongly mixed (Table S1).

The σ_1 and π^* orbitals of SAS are schematically depicted in Scheme 3, for which the molecular plane is defined by the six Si atoms (see ref. [33] for a definition of σ and π character and treatment of chains that do not have a plane of symmetry).

2.4. Calculated Transitions in Free-Chain Permethylated n -Hexasilane 4

The effects of varying the three SiSiSiSi dihedral angles in n -hexasilanes on the excited states were analyzed by using n -Si₆Me₁₄ in the conformation given in Scheme 2. In these structures, one dihedral angle was varied from $\omega = 0$ to 180° ,

Table 1. Observed^[a] and calculated electronic transitions in hexasilanes **1** (SAS-2, C), **2** (AAS, C₁), and **3** (AEA-3, C₂).

Compd	Exptl $\tilde{\nu}$ [10 ³ cm ⁻¹]	<i>f</i>	<i>D</i> [Debye ²]	<i>B</i> [De- bye ² β _e 10 ⁴ cm ⁻¹]	SAC-CI Symmetry	$\tilde{\nu}$ [10 ³ cm ⁻¹]	<i>f</i>	Assignment ^[b]	Symmetry	TD-PBE0 $\tilde{\nu}$ [10 ³ cm ⁻¹]	<i>f</i>	Assignment ^[b]	
1	41.1	0.10	5.4	7.0	A _u	41.5	0.18	H→L	σ ₁ σ* A _u	43.4	0.05	H→L	σ ₁ π* L+1
	41.9	0.10	5.1	-13	A _u	42.1	0.20	H→L+1	σ ₁ π* A _u	43.9	0.22	H→L	σ ₁ σ*
	45.3	0.25	12	23	A _u	44.8	0.15	H-2→L	σ ₃ σ* A _u	45.4	0.14	H-1→L	σ ₂ σ*
					A _g	45.6	0.00	H→L+2	σ ₁ π ₂ * A _g	45.8	0.00	H-2→L	σ ₃ σ*
	49.1	0.0085	0.37	-0.68	A _u	46.6	0.01	H-2→L+1	σ ₃ π* A _g	46.3	0.00	H-2→L	σ ₃ σ*
					A _g	46.7	0.00	H-1→L	σ ₂ π* A _u	46.6	0.01	H-1→L+1	σ ₂ π*
					A _g	48.3	0.00	H→L+2	σ ₁ π ₂ * A _g	47.6	0.00	H→L+2	σ ₁ π ₂ *
	[50.7 ^[d]]	1.36	57	26]									
2	39.0	0.24	13	1.6	A	37.4	0.61	H→L	σ ₁ σ* A	40.9	0.58	H→L	σ ₁ σ*
	40.6	0.13	6.8	0.15	A	41.5	0.03	H→L+1	σ ₁ π* A	43.5	0.03	H→L+1	σ ₁ π*
	44.3	0.20	9.7	8.2	A	44.2	0.02	H-2→L	σ ₂ σ* A	44.5	0.02	H-1→L	σ ₂ σ*
					A	45.7	0.02	H-1→L	σ ₃ σ* A	46.1	0.001	H-2→L	σ ₃ σ*
	45.8	0.028	1.3	3.9	A	47.4	0.03	H-1→L+1	σ ₂ π* A	47.3	0.004	H-1→L+1	σ ₂ π*
					A	47.7	0.004	H-3→L	σ ₄ σ* A	47.9	0.005	H-3→L	σ ₄ σ*
					A	48.9	0.007	H→L+3	σ ₁ π* A	48.0	0.004	H→L+2	σ ₁ π*
	[51.7 ^[d]]	1.16	48	36]									
3	38.9	0.15	8.2	4.3	B	36.9	0.79	H→L	σ ₁ σ* B	39.6	0.75	H→L	σ ₁ σ*
	39.5	0.38	20	4.3	A	41.7	0.01	H→L+1	σ ₁ π* ^[c] A	43.4	0.002	H→L+1	σ ₁ π*
	42.2	0.014	0.72	-3.1	A	43.6	0.01	H-1→L	σ ₂ σ* A	44.4	0.02	H-1→L	σ ₂ σ*
					B	44.0	0.01	H-2→L	σ ₃ σ* B	45.6	0.01	H-2→L	σ ₃ σ*
					A	47.0	0.01	H-3→L	σ ₄ σ* A	46.3	0.00	H-3→L	σ ₄ σ*
	44.7	0.15	7.2	3.4	B	48.5	0.22	H-1→L+1	σ ₂ π* ^[c] B	47.1	0.18	H→L+3	σ ₁ σ*
	48.1	0.055	2.4	13	A	49.2	0.03	H-2→L+1	σ ₃ π* A	47.6	0.00	H→L+2	σ ₁ σ*
		[54.9 ^[d]]	1.62	63	27]								

[a] Absorption and MCD in 3-MP, LD in stretched polyethylene. [b] H and L represent HOMO and LUMO, respectively. H-1 and H-2 are interchanged in Hartree-Fock and DFT. [c] The terminating MO of this transition is of strongly mixed σ and π character (Table S1). [d] Probably due to solvent.

whereas the other two were restricted at *syn* ($\omega=0^\circ$) or *anti* ($\omega=180^\circ$). Thus, these conformational changes represent the structural changes in 1) SAS to AAS (ω_1), 2) AAS to AAA (ω_3), and 3) ASA to AAA (ω_2). The variation in the excitation energy and oscillator strength of *n*-Si₆Me₁₄ as a function of the angles ω_1 , ω_3 , and ω_2 is displayed in Figures 3, 4, and 5, respectively. The ground-state potential energy curves along these conformational changes are shown in Figure S7. The energy variation along these dihedral angles relative to the most stable ground-state conformation is less than 1.0 kcal mol⁻¹ in the $\omega=30$ – 180° range.

To understand the behavior of the low-lying $\sigma\pi^*$ and $\pi\pi^*$ transitions as the dihedral angle changes, the variation in the orbital energy levels of HOMO-1 to LUMO+1 was examined. The orbital energy changes for the ω_1 , ω_3 , and ω_2 variations are plotted in Figure 6A–C together with schematic orbital shapes. Orbital back lobes are shown only if relevant to the understanding of orbital interactions. More complete views of the MOs for dihedral angles $\omega=0$, 90 , and 180° are collected in Figures S8–S10.

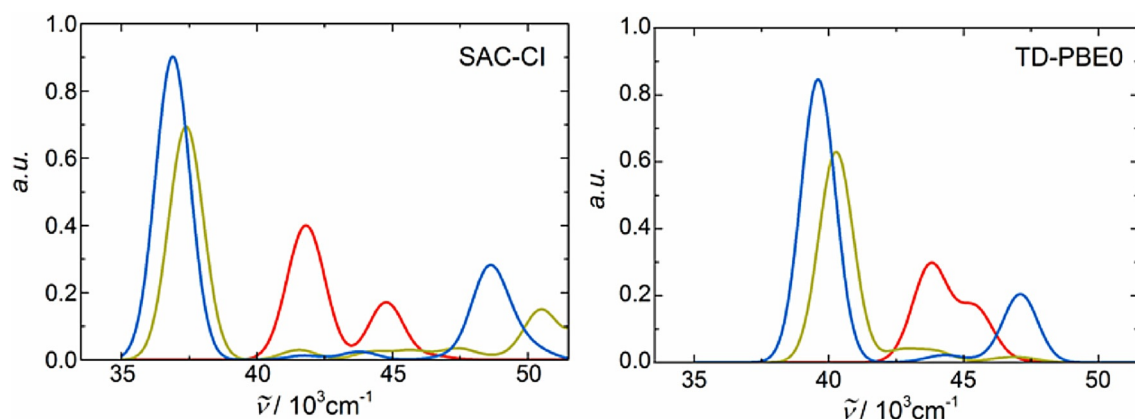
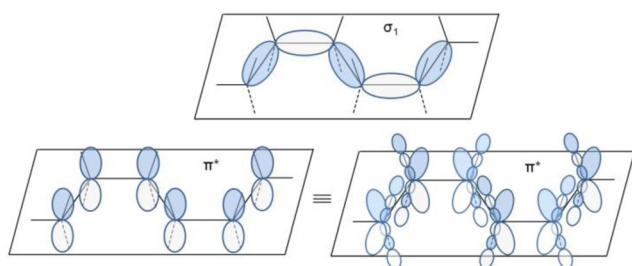


Figure 2. Calculated absorption spectra of **1** (SAS; red), **2** (AAS; dark yellow), and **3** (AEA; blue) with Gaussian convolution (FWHM of 1500 cm^{-1}). Left, SAC-CI; right, TD-DFT/PBE0.



Scheme 3. Schematic representations of orbitals of SAS: σ_1 and π^* , excluding and including contributions from the lateral substituents

3. Discussion

Although the spectra of hexasilanes **1–3** are poorly resolved, the simultaneous fitting of the UV, MCD, and LD_r spectra allows their decomposition into a series of four electronic transitions with a fair degree of confidence, although additional weak transitions could, of course, be present. The existence of the fifth very intense transition that is present in all three hexasilanes above $50\,000\text{ cm}^{-1}$ is questionable, as it lies at the very edge of the spectral window dictated by the solvents used, 3-MP and polyethylene, and it could well be an artifact due to an incompletely subtracted onset of solvent signals. We list this possible fifth transition, as it is required for the fitting of the observed spectral curves, but we shall de-emphasize it in the following. Given that diffuse basis set functions were not included in our calculations, the computed results are also unreliable in this region.

The assignments of electronic transitions in the spectra are facilitated by the generally good agreement between calculations and experiment, but some uncertainties remain, mostly due to the congestion in both the observed and the calculated spectra. We shall rely primarily on the results of the SAC-CI computations, but similar transitions, albeit at somewhat higher energies, were also obtained by the TD-PBE0 method.

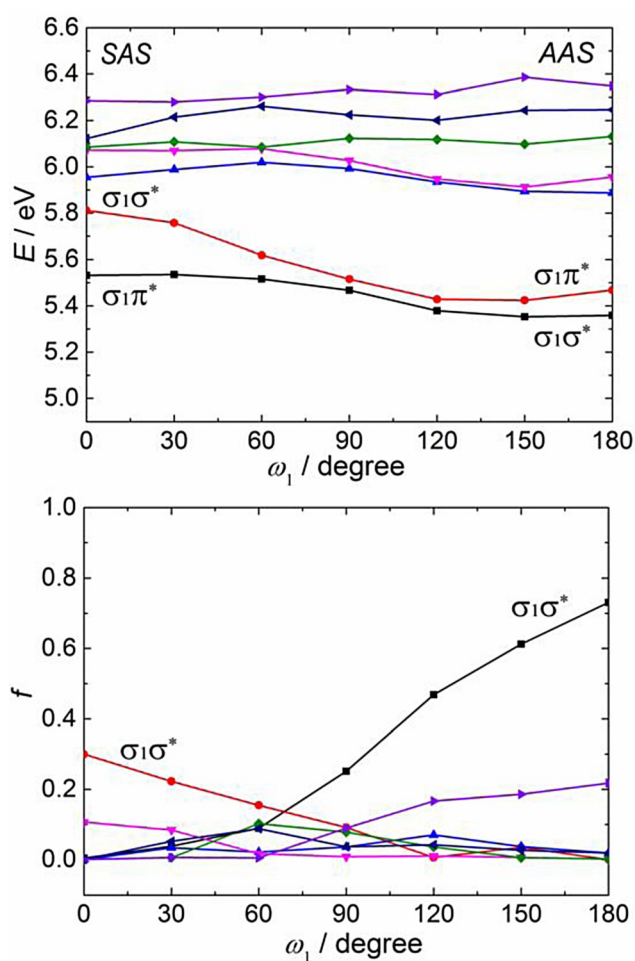


Figure 3. TD-PBE0 transition energy and oscillator strength of $n\text{-Si}_6\text{Me}_{14}$ with $\omega_1 = 0\text{--}180^\circ$, $\omega_2 = 180^\circ$, and $\omega_3 = 0^\circ$.

3.1. The Spectra of **1–3**

Ignoring the strong absorption at the edge of the observed region as noted above, the simultaneous fits of the room-temperature UV, MCD, and LD_r spectra of **1–3** suggest the presence of four transitions in the reliably observed region up to

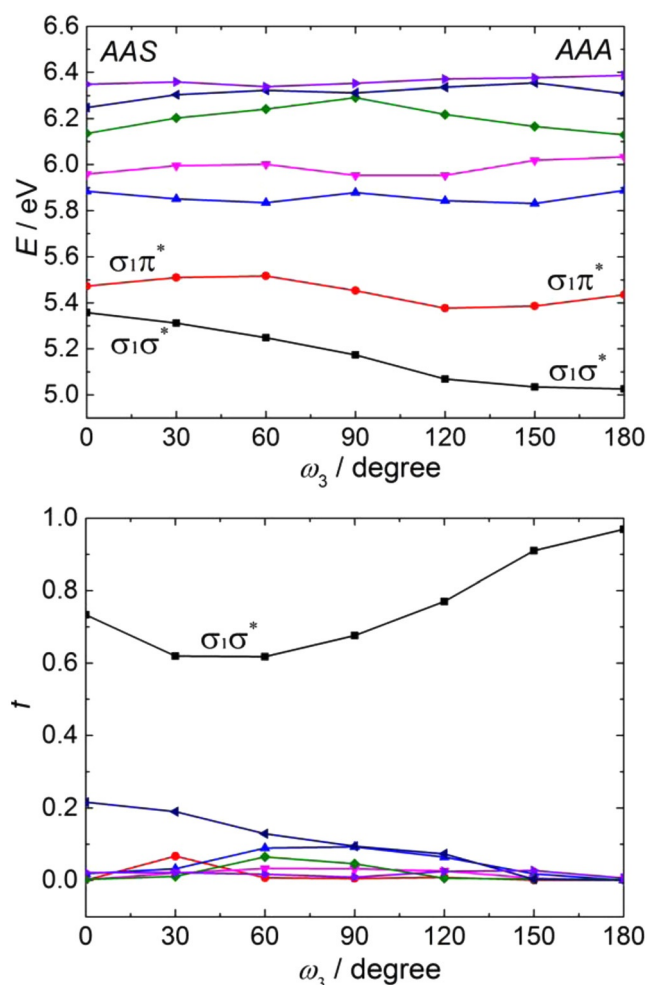


Figure 4. TD-PBE0 transition energy and oscillator strength of $n\text{-Si}_6\text{Me}_{14}$ with $\omega_1 = 180^\circ$, $\omega_2 = 180^\circ$, and $\omega_3 = 0\text{--}180^\circ$.

nearly 50000 cm^{-1} (Table 1) and additional weak ones may be present as well. The assignment of these transitions to the calculated ones is complicated by the existence of several low-energy conformations predicted for **1** and **3**. Their presence does not pose a substantial problem in the case of **3**, even though the ground-state energies of its four conformers are calculated to lie within 1 kcal mol^{-1} of each other (Table S4), as the spectra calculated for all four by the SAC-CI and TD-DFT methods are very similar (Tables S7 and S8) and virtually all the absorption intensity is located in the first transition. It is immaterial which conformer one chooses for the comparison of calculated and observed spectra, and in Table 1 we chose AEA-3 in C_2 structure.

3.1.1. Spectrum of **1**

In this case, according to the SAC-CI method the optimized geometries lie in a region in which crossing of the lowest two excited states, both of A_u symmetry, is avoided. The configurations involved in the mixing are $\sigma_{1\sigma^*}$ and $\sigma_{1\pi^*}$, for which only the former contributes significant oscillator strength. The computed intensities of transitions into the two states depend

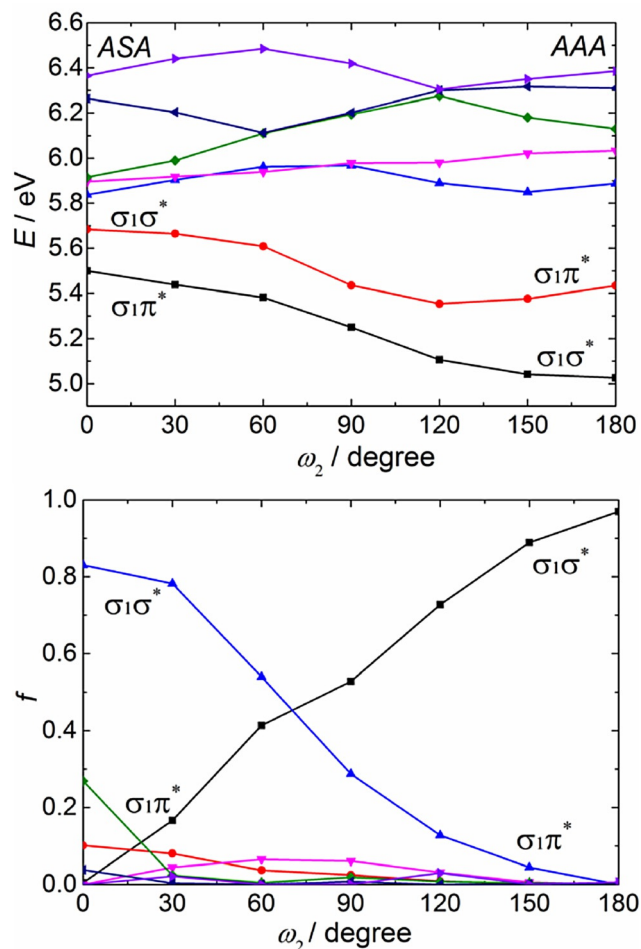


Figure 5. TD-PBE0 transition energy and oscillator strength of $n\text{-Si}_6\text{Me}_{14}$ with $\omega_1 = 180^\circ$, $\omega_2 = 0\text{--}180^\circ$, and $\omega_3 = 180^\circ$.

strongly on the choice of conformation. The observed intensities of these transitions are similar (Table 1), $f = 0.1$ both at 41100 and 41900 cm^{-1} . The B terms in the MCD spectrum of **1** have opposite signs, and this confirms that both fitted Gaussians indeed belong to distinct electronic transitions. The similar intensities of the two first bands agree with the SAC-CI results for the conformation SAS-2, which was chosen for Table 1. They do not agree with SAC-CI results for conformation SAS-1, computed to be 1.1 kcal mol^{-1} more stable than SAS-2, as these results predict the second transition to be much more intense than the lowest one, nor for conformation SAS-3, computed to be 1.5 kcal mol^{-1} less stable than SAS-2 and predicted to have an intense second transition and virtually no intensity in the first (Table S5). To complicate matters further, TD-DFT calculations (Table S6) position the region of the avoided crossing somewhat differently and place, by far, most of the intensity into the second transition for conformers SAS-1 and SAS-2 and into the first transition for conformer SAS-3.

We do not believe that the relative ground-state energies of the conformers are computed sufficiently reliably to decide which one or ones are observed. The comparable observed intensities leave little doubt that the computations are correct in

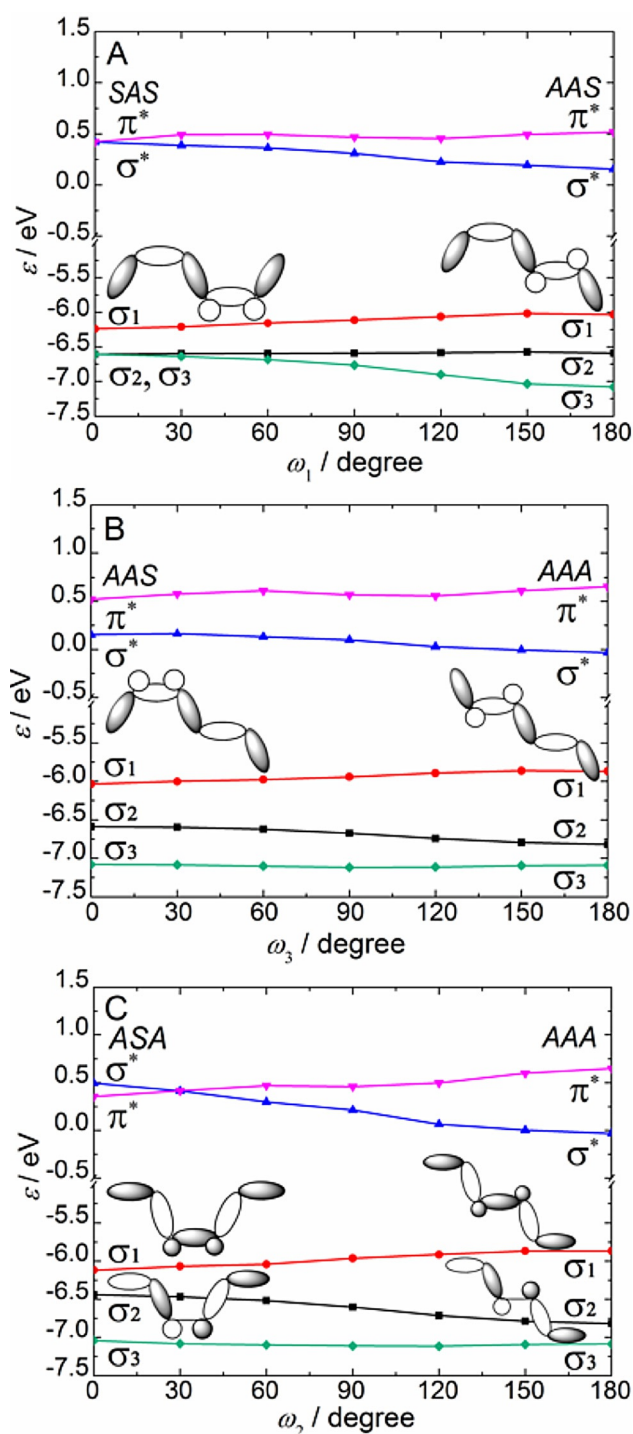


Figure 6. PBE0 orbital energy levels and schematic orbitals for HOMO–1 to LUMO + 1 in $n\text{-Si}_6\text{Me}_{14}$ with A) $\omega_1 = 0\text{--}180^\circ$, $\omega_2 = 180^\circ$, $\omega_3 = 0^\circ$; B) $\omega_1 = 180^\circ$, $\omega_2 = 180^\circ$, $\omega_3 = 0\text{--}180^\circ$; and C) $\omega_1 = 180^\circ$, $\omega_2 = 0\text{--}180^\circ$, $\omega_3 = 180^\circ$. The back lobes are depicted only if relevant to understanding orbital interactions.

that the dominant conformer or conformers have a geometry that lies in the region of an avoided crossing of the first two excited states, both of which have a mixed $\sigma_1\sigma^*$ and $\sigma_1\pi^*$ character. The computed transition moment directions, although not very different (Table S9), are sufficiently far from parallel that magnetic mixing of the two states can credibly give rise

to the opposite B terms observed. The negative B term of the second excited state apparently gains further strength from magnetic mixing with the state at 45300 cm^{-1} , which carries considerable intensity.

The broad and intense ($f=0.25$) third observed band centered at 45300 cm^{-1} is assigned to the next transition into an A_u symmetry $\sigma_3\sigma^*$ state calculated at 44800 cm^{-1} . Three additional forbidden transitions into states of A_g symmetry are calculated to be present in this general region but are not observed. Finally, a weak fourth transition with a negative B term is observed at 49100 cm^{-1} and is assigned to a $\sigma_3\pi^*$ transition into a state of A_u symmetry, calculated at 46600 cm^{-1} .

3.1.2. Spectrum of 2

Due to the lower symmetry of **2**, we lose the useful classification of the computed excited states into two distinct symmetry classes, and only the distinction of partial σ and π character by using the definitions^[33] based on NHOs obtained from natural bond orbital analysis remains (Table S1). The first band of **2** observed at 39000 cm^{-1} ($f=0.24$) is readily assigned to the $\sigma_1\sigma^*$ transition calculated at 37400 cm^{-1} ($f=0.61$). Beyond this point, the observations do not agree with the results of the calculations. In the absorption spectrum, two strong bands are observed at 40600 and 44300 cm^{-1} with $f=0.13$ and 0.20 , respectively, and a weak one at 45800 cm^{-1} with $f=0.03$. The calculations suggest the presence of four transitions of comparable f values of $0.02\text{--}0.03$, followed by a pair of much weaker transitions unlikely to be observed. It is not clear how to reconcile the two sets of results and to assign the observed transitions to the calculated transitions.

It is improbable that the second observed band is merely a reflection of a non-Gaussian shape of the first transition and that it should be added to the first band, even though such an assignment would improve the agreement of observed and computed oscillator strengths. The two bands have distinctly different linear dichroism and, even more important, the intensities of their MCD signals differ by a factor of ten. In all probability, these are indeed two different transitions. We note that unlike the second B terms of **1** and **3**, the second B term in **2** has a positive sign.

The disagreement is puzzling, as the computational methods used seem to perform well for **1** and **3** and even the first transition in **2**. An obvious possible explanation is an inadequacy of the method used for geometry optimization, especially for the central dihedral angle. If the real geometry lies in an area of an avoided crossing similar to that in **1**, the resulting configuration mixing could spread oscillator strength from one transition to others. Conceivably, more than one conformer could also be present. In summary, although we consider the experimental results for **2** dependable, the present computational results for this hexasilane are not useful.

3.1.3. Spectrum of 3

This hexasilane is calculated to have four conformations of nearly equal ground-state energy. As pointed out above, the

computed spectra are all alike, and for Table 1 we chose one of the C_2 symmetry conformations (AEA-3, Table S4). For the first excitation, we propose that both Gaussian components at 38900 and 39500 cm^{-1} (total oscillator strength $f=0.53$) should be attributed to a single $\sigma_1\sigma^*$ transition, calculated at 36900 cm^{-1} with $f=0.79$. This assignment fits the LD_r data, but an argument against it is that MCD intensity is similar for the two components, whereas the absorption intensity is different by a factor of 2.5. This would imply somewhat different shapes in the absorption and MCD spectra, and this is apparent in Figure S3. The discrepancy is small and appears acceptable.

The next band observed at 42200 cm^{-1} ($f=0.01$) is assigned to a $\sigma_1\pi^*$ transition calculated at 41700 cm^{-1} ($f=0.01$). This is considerable intensity for a $\sigma_1\pi^*$ transition to a state of *A* symmetry in the C_2 point group, but the terminating π^* orbital has a strong σ^* admixture (Table S1). The following band, observed at 44700 cm^{-1} ($f=0.15$), is assigned to a *B* symmetry state of $\sigma_2\pi^*$ nature (the π^* MO contains a large admixture of σ character, cf. Table S1), calculated at 48500 cm^{-1} ($f=0.22$). This attribution is somewhat uncertain, as three additional weak transitions with f values of 0.01–0.02 are predicted by SAC-Cl at slightly lower energies and are presumably buried under the more intense transition. Finally, a weak ($f=0.06$) fourth transition is observed at 48100 cm^{-1} and is tentatively assigned as a $\sigma_3\pi^*$ transition to a state of *A* symmetry calculated at 49200 cm^{-1} ($f=0.03$).

3.1.4. Comparison of the Spectra of 1–3

Comparing all three spectra, in both **2** (AAS) and **3** (AEA), the most easily identified lowest energy intense absorption band is redshifted by about 2000 cm^{-1} relative to that of **1** (SAS) and is intensified by a factor of 2.5 and 5, respectively (Figure 1). This behavior is qualitatively reproduced by the SAC-Cl method; the first bands are calculated at 37400 and 36900 cm^{-1} with oscillator strengths of $f=0.61$ and 0.79 for **2** and **3**, respectively, compared to the values of 41500 and 42100 cm^{-1} and $f=0.18$ and 0.20 calculated for **1**. The same trend with respect to the variation in the absorption energy is also calculated for *n*-Si₆Me₁₄ (**4**); SAS-AAS (Figure 3) and AAS-AAA (Figure 4). The origin of the redshift is the destabilization of the σ_1 orbital and stabilization of the σ^* orbital as the dihedral angle increases (Figure 6). Frontier MOs of **1**, **2**, and **3** are similar to those of the corresponding MOs of *n*-Si₆Me₁₄ in the SAS, AAS, and AEA conformations, respectively. Figure 2 shows that the TD-DFT method performs less well in that it exaggerates the differences between the first bands of the three compounds and fails to account for the nearly identical first excitation energies of **2** and **3**.

In summary, the computed spectra of **1–3** appear to be characterized by a nearly degenerate pair of excitations from the HOMO, σ_1 , to the lowest unoccupied MOs of σ and π symmetry (σ^* and π^*) at about 40000 cm^{-1} , with the former strong and the latter weak, followed by another nearly degenerate pair of similar but weaker transitions from the HOMO–1 (σ_2) roughly 5000 cm^{-1} higher, plus additional weak transitions. These results are nicely compatible with the experimental ob-

servations for **1** and **3**, and in the case of the first transition, also for **2**, but many of the expected very weak transitions remain unobserved. The detailed arrangement of the computed transition energies and intensities is determined by the conformation of the silicon backbone, and this will be systematically investigated next.

3.2. The Spectra of 4

The three types of variations in the dihedral angles (ω_1 – ω_3) in *n*-Si₆Me₁₄ (**4**) that were examined are instructive for seeing how conformation control affects the optical properties of *n*-hexasilanes (Figures 3–5).

We first focus on variation in the angle ω_1 (Figure 3). At $\omega_1=0^\circ$ (SAS), the S_1 state is reached by a $\sigma\pi^*$ excitation and the nearby S_2 state is reached by a $\sigma\sigma^*$ excitation. If ω_1 is increased, symmetry is lowered. The S_1 and S_2 states are still represented by these two configurations, which now mix. The $\sigma\sigma^*$ component carries a large oscillator strength, and the $\sigma\pi^*$ component carries only a small one; the oscillator strength of transitions into the two states depends on their ratio. They undergo an avoided crossing at around $\omega_1=60^\circ$, as seen in the variation in the oscillator strength. At the AAS ($\omega_1=180^\circ$) conformation, symmetry is reestablished, and the S_1 state is reached by a $\sigma\sigma^*$ excitation with a strong oscillator strength of $f=0.7$. The response of the low-energy part of the spectrum to the variation in the dihedral angle ω_1 is thus dictated by the interchange in the order of the $\sigma\pi^*$ and $\sigma\sigma^*$ excitations and in that sense is strongly reminiscent of the conformational response of the spectrum of *n*-tetrasilane.^[9,35]

The energies of both transitions drop as the conformation changes from SAS to AAS. The energy of the $\sigma\sigma^*$ transition is lowered by 0.45 eV, from 5.81 to 5.36 eV, and that of the $\sigma\pi^*$ transition is lowered by 0.07 eV, from 5.54 to 5.47 eV, which agrees well with the trend found in peralkylated hexasilanes **1** (SAS) and **2** (AAS). This trend can be qualitatively understood as being due to σ and σ^* orbital energy changes (Figure 6A).

Among the higher states, in SAS ($\omega_1=0^\circ$), which is close to the conformation of **1** with absorptions at 45300 and 49100 cm^{-1} , transition to the S_4 state, characterized as $\sigma_3\sigma^*$, has considerable oscillator strength. In AAS ($\omega_1=180^\circ$), which corresponds to **2** with the absorption band in the higher energy region, transition to the S_6 state has a large oscillator strength. Other transitions do not have notable intensity.

Next, we consider the conformational change from AAS to AAA by a variation in the dihedral angle ω_3 , while the other angles are fixed at $\omega_1=\omega_2=180^\circ$ (Figure 4). Now, the energy of the $\sigma_1\sigma^*$ configuration lies below that of the $\sigma_1\pi^*$ configuration at AAS, AAA, and all intermediate geometries. The energies of the S_1 and S_2 states are well separated, and mixing of the dominant $\sigma\sigma^*$ and $\sigma\pi^*$ configurations is small at all geometries. There is no avoided crossing, and the transition to the S_1 state is always intense. At the AAA conformation ($\omega_1=180^\circ$), only the S_1 state has a large oscillator strength ($f\approx 1.0$) and those of all other transitions are nearly zero, which shows that the $\sigma_1\sigma^*$ configuration is significant in the S_1 state. Transitions to the S_2 and S_3 states have weak intensity ($f<0.1$) all along

this ω_3 variation. In brief, the variation in the dihedral angle ω_3 is expected to produce no dramatic spectral changes other than a significant drop in the energy of the first transition as one proceeds from AAS to AAA and in that regard is very different from the variation in ω_1 .

Finally, during the conformational change from ASA to AAA by varying the angle ω_2 (Figure 5), the $S_1(1B)$ and $S_2(2B)$ states undergo an avoided crossing and interchange their character ($\sigma\sigma^*$, $\sigma\pi^*$), even though they are separated by about 0.2 ($\omega_2 = 0^\circ$) and 0.4 eV ($\omega_2 = 180^\circ$). Their oscillator strengths change drastically as their contents of the $\sigma\sigma^*$ component change during the process. The situation is thus very similar to that encountered with the variation in the angle ω_1 . At $\omega_2 = 120^\circ$, the conformation and the expected spectra correspond to **3** (AEA). The ASA conformation shows strong absorption only in the high energy region, above 5.8 eV.

A rationalization of the effects of conformational changes in the low-energy part of the spectra thus follows from the knowledge of the relative energies of the lowest $\sigma_1\sigma^*$ and $\sigma_1\pi^*$ configurations. Given that the energy of the $\sigma_1\pi^*$ configuration is almost independent of the conformation (Figures 3–5), the conformational behavior of the spectra is primarily determined by the effect of dihedral angles on the energy of the lowest $\sigma_1\sigma^*$ configuration. This can be understood in terms of the energies of the σ_1 MO and the lowest σ^* MO and, thus, ultimately in terms of the extremely simple Ladder C model.^[37,49] In this model, relative energies of conformations are dictated solely by the vicinal (1,4) resonance integrals between NHOs located at the Si atoms of the bond that is being twisted. At a dihedral angle of 0° (*syn*), this resonance integral is negative; near a dihedral angle of 90° , it goes through zero; at a dihedral angle of 180° , it is positive. Combined with the knowledge of signs of the coefficients of the NHOs in the σ and σ^* MOs, this permits first-order perturbation theory estimates of the effect of dihedral angle changes on the energies of these orbitals. Note that the change in the sign of the resonance integral is due to the π component of the overlap of the vicinal NHOs, and in that sense, the conformational isomerization of a saturated chain is clearly related to the geometrical *cis/trans* isomerization of a double bond.

These arguments show that as the angle ω_1 increases (Figure 6A), the σ_1 orbital (HOMO) should be destabilized and the σ^* orbital should be stabilized, and this rationalizes the strong drop in the $\sigma\sigma^*$ transition energy from SAS to AAS and the change in the order of energies of the lowest $\sigma_1\sigma^*$ and $\sigma_1\pi^*$ configurations. In contrast, as the angle ω_3 is increased (Figure 6B), further destabilization of the σ MO and stabilization of the σ^* MO merely lowers the energy of the already lowest $\sigma_1\sigma^*$ configuration. It causes no changes in the order of the $\sigma\sigma^*$ and $\sigma\pi^*$ configurations and the transition to the S_1 state drops in energy but keeps its strong oscillator strength throughout. Finally, if ω_2 is increased (Figure 6C), the changes in the σ_1 and σ^* energies are very similar to those seen in Figure 6A and are rationalized in the same way. They once again lead to an interchange of the $\sigma\sigma^*$ and $\sigma\pi^*$ nature of the lowest two transitions, an avoided crossing, and dramatic ef-

fects on transition intensities, in addition to a change in the energy of the first transition.

4. Summary

The electronic excited states of three conformationally controlled peralkylated *n*-hexasilanes **1–3** (SAS, AAS, and AEA; S = *syn*, A = *anti*, E = *eclipsed*) were investigated by using UV, MCD, and LD spectroscopy. Simultaneous decomposition of the three types of spectra into Gaussian contributions played a key role in the assignment of the individual electronic transitions and determination of their wavenumbers, oscillator strengths, and MCD *B* terms. SAC-CI and DFT/PBE0 calculations were used to analyze the nature of the observed excitations. They provided useful results for hexasilanes **1** and **3**, but not for **2**. The striking dependence of the energy and intensity of the first intense transition, located near $40\,000\text{ cm}^{-1}$, on the silicon backbone conformation was found to result from changes in the energies of the σ_1 and σ^* orbitals, which could be understood in very simple terms. The conformational dependence of the excitation energies and transition properties was examined more generally on the free chain *n*-Si₆Me₁₄ in various combinations of dihedral angles. An avoided crossing between the $\sigma\sigma^*$ and $\sigma\pi^*$ states was found to occur in the SAS-AAS and ASA-AAA conformational transformations and caused dramatic differences in the transition intensities.

Acknowledgements

M.E. acknowledges financial support from a Grant-in-Aid for Scientific Research from the Japan Society for the Promotion of Science (JSPS) and Nanotechnology Platform Program (Molecule and Material Synthesis) of the Ministry of Education, Culture, Sports, Science, and Technology of Japan (MEXT). The computations were partly performed by using the Research Center for Computational Science in Okazaki, Japan. The work in Boulder was supported by the US National Science Foundation (CHEM-1566435). Work in Prague was supported by the Institute of Organic Chemistry and Biochemistry (RVO:61388963).

Keywords: configuration interaction · density functional calculations · magnetic circular dichroism · oligosilanes · UV/Vis spectroscopy

- [1] H. Gilman, W. H. Atwell, G. L. Schwebke, *Chem. Ind.* **1964**, 1063.
- [2] H. Gilman, W. H. Atwell, G. L. Schwebke, *J. Organomet. Chem.* **1964**, *2*, 369–371.
- [3] H. Sakurai, M. Kumada, *Bull. Chem. Soc. Jpn.* **1964**, *37*, 1894.
- [4] D. N. Hague, R. H. Prince, *Chem. Ind. (London)* **1964**, 1492.
- [5] K. Obata, M. Kira, *Organometallics* **1999**, *18*, 2216–2222.
- [6] H. A. Fogarty, R. Imhof, J. Michl, *Proc. Natl. Acad. Sci. USA* **2004**, *101*, 10517–10522.
- [7] M. K. Raymond, Ph.D. Dissertation, University of Colorado, Boulder, CO, **1997**.
- [8] H. A. Fogarty, Ph.D. Dissertation, University of Colorado, Boulder, CO **2005**.
- [9] H. Tsuji, H. A. Fogarty, M. Ehara, R. Fukuda, D. L. Casher, K. Tamao, H. Nakatsuji, J. Michl, *Chem. Eur. J.* **2014**, *20*, 9431–9441.

- [10] S. Mazières, M. K. Raymond, G. Raabe, A. Prodi, J. Michl, *J. Am. Chem. Soc.* **1997**, *119*, 6682–6683.
- [11] D. J. Williams, *Angew. Chem. Int. Ed. Engl.* **1984**, *23*, 690–703; *Angew. Chem.* **1984**, *96*, 637–651.
- [12] H. Kishida, T. Hasegawa, Y. Iwasa, T. Koda, Y. Tokura, *Phys. Rev. Lett.* **1993**, *70*, 3724–3727.
- [13] R. G. Kepler, Z. G. Soos in *Primary Photoexcitations in Conjugated Polymers* (Ed.: N. S. Sariciftci), World Scientific, Singapore, **1997**, pp. 363–383.
- [14] M. Kumada, K. Tamao, *Adv. Organomet. Chem.* **1968**, *6*, 19–117.
- [15] R. D. Miller, J. Michl, *Chem. Rev.* **1989**, *89*, 1359–1410.
- [16] M. Kira, T. Miyazawa in *The Chemistry of Organic Silicon Compounds, Vol. 2* (Eds.: Z. Rappoport, Y. Apeloig), Wiley, Chichester, **1998**, p. 1311.
- [17] J. Michl, R. West in *Silicon Containing Polymers* (Eds.: R. G. Jones, W. Ando, J. Chojnowski), Kluwer Academic, Dordrecht, **2000**, p. 499.
- [18] R. West in *The Chemistry of Organic Silicon Compounds, Vol. 3* (Eds.: Z. Rappoport, Y. Apeloig), Wiley, Chichester, **2001**, p. 541.
- [19] H. A. Fogarty, D. L. Casher, R. Imhof, T. Schepers, D. W. Rooklin, J. Michl, *Pure Appl. Chem.* **2003**, *75*, 999–1020.
- [20] H. Tsuji, J. Michl, A. Tshimitsu, K. Tamao, *J. Synth. Org. Chem. Jpn.* **2002**, *60*, 762–773.
- [21] H. Tsuji, J. Michl, K. Tamao, *J. Organomet. Chem.* **2003**, *685*, 9–14.
- [22] L. A. Harrah, J. M. Zeigler, *J. Polym. Sci. Polym. Lett. Ed.* **1985**, *23*, 209–211.
- [23] P. Trefonas, J. R. Damewood, R. West, R. D. Miller, *Organometallics* **1985**, *4*, 1318–1319.
- [24] T. Gahimer, W. J. Welch, *Polymer* **1996**, *37*, 1815–1823.
- [25] T. Sanji, K. Sakamoto, H. Sakurai, K. Ono, *Macromolecules* **1999**, *32*, 3788–3794.
- [26] S. S. Bukalov, L. A. Leites, R. West, *Macromolecules* **2001**, *34*, 6003–6004.
- [27] K. Obata, M. Kira, *RIKEN Rev.* **1995**, *11*, 39–40.
- [28] H. A. Fogarty, C. H. Ottosson, J. Michl, *J. Mol. Struct.* **2000**, *556*, 105–121.
- [29] H. A. Fogarty, C. H. Ottosson, J. Michl, *J. Mol. Struct.* **2000**, *506*, 243–255.
- [30] J. Michl, R. West, *Acc. Chem. Res.* **2000**, *33*, 821–823.
- [31] H. A. Fogarty, C. H. Ottosson, J. Michl, *J. Phys. Chem. B* **2006**, *110*, 25485–25495.
- [32] H. Tsuji, M. Terada, A. Tshimitsu, K. Tamao, *J. Am. Chem. Soc.* **2003**, *125*, 7486–7487.
- [33] A. Bande, J. Michl, *Chem. Eur. J.* **2009**, *15*, 8504–8517.
- [34] R. Crespo, M. C. Piqueras, J. Michl, *Theor. Chem. Acc.* **2007**, *118*, 81–87.
- [35] H. Teramae, J. Michl, *Mol. Cryst. Liq. Cryst.* **1994**, *256*, 149–159.
- [36] H. S. Plitt, J. W. Downing, M. K. Raymond, V. Balaji, J. Michl, *J. Chem. Soc. Faraday Trans.* **1994**, *90*, 1653–1662.
- [37] T. Schepers, J. Michl, *J. Phys. Org. Chem.* **2002**, *15*, 490–498.
- [38] F. Neumann, H. Teramae, J. W. Downing, J. Michl, *J. Am. Chem. Soc.* **1998**, *120*, 573–582.
- [39] B. Albinsson, D. Antic, F. Neumann, J. Michl, *J. Phys. Chem. A* **1999**, *103*, 2184–2196.
- [40] C. H. Ottosson, J. Michl, *J. Phys. Chem. A* **2000**, *104*, 3367–3380.
- [41] R. West, *J. Organomet. Chem.* **2003**, *685*, 6–8.
- [42] S. Ohashi, Y. Naruse, S. Inagaki, *J. Organomet. Chem.* **2003**, *682*, 119–122.
- [43] R. Crespo, H. Teramae, D. Antic, J. Michl, *Chem. Phys.* **1999**, *244*, 203–214.
- [44] R. Crespo, M. Merchan, J. Michl, *J. Phys. Chem. A* **2000**, *104*, 8593–8599.
- [45] M. C. Piqueras, M. Merchan, R. Crespo, J. Michl, *J. Phys. Chem. A* **2002**, *106*, 9868–9873.
- [46] B. Albinsson, H. Teramae, J. W. Downing, J. Michl, *Chem. Eur. J.* **1996**, *2*, 529–538.
- [47] M. C. Piqueras, R. Crespo, J. Michl, *J. Phys. Chem. A* **2003**, *107*, 4661–4668.
- [48] D. W. Rooklin, T. Schepers, M. K. Raymond-Johansson, J. Michl, *Photochem. Photobiol. Sci.* **2003**, *2*, 511–517.
- [49] H. S. Plitt, J. Michl, *Chem. Phys. Lett.* **1992**, *198*, 400–405.
- [50] R. Imhof, H. Teramae, J. Michl, *Chem. Phys. Lett.* **1997**, *270*, 500–505.
- [51] R. Imhof, D. Antic, D. E. David, J. Michl, *J. Phys. Chem. A* **1997**, *101*, 4579–4586.
- [52] H. A. Fogarty, H. Tsuji, D. E. David, C. H. Ottosson, J. Michl, K. Tamao, M. Ehara, H. Nakatsuji, *J. Phys. Chem. A* **2002**, *106*, 2369–2373.
- [53] K. Tamao, H. Tsuji, M. Terada, M. Asahara, S. Yamaguchi, A. Tshimitsu, *Angew. Chem. Int. Ed.* **2000**, *112*, 3425–3428; *Angew. Chem.* **2000**, *112*, 3567–3570.
- [54] H. Tsuji, A. Tshimitsu, K. Tamao, J. Michl, *J. Phys. Chem. A* **2001**, *105*, 10246–10248.
- [55] S. Seki, K. Okamoto, Y. Matsui, S. Tagawa, H. Tsuji, A. Tshimitsu, K. Tamao, *Chem. Phys. Lett.* **2003**, *380*, 141–145.
- [56] H. Mallesha, H. Tsuji, K. Tamao, *Organometallics* **2004**, *23*, 1639–1642.
- [57] H. Tsuji, A. Fukazawa, S. Yamaguchi, A. Tshimitsu, K. Tamao, *Organometallics* **2004**, *23*, 3375–3377.
- [58] A. Fukazawa, H. Tsuji, K. Tamao, *J. Am. Chem. Soc.* **2006**, *128*, 6800–6801.
- [59] R. Tanaka, M. Unno, H. Matsuoto, *Chem. Lett.* **1999**, 595–596.
- [60] I. El-Sayed, Y. Hatanaka, C. Muguruma, S. Shimada, M. Tanaka, N. Koga, M. Mikami, *J. Am. Chem. Soc.* **1999**, *121*, 5095–5096.
- [61] I. El-Sayed, Y. Hatanaka, S. Onozawa, M. Tanaka, *J. Am. Chem. Soc.* **2001**, *123*, 3597–3598.
- [62] Y. Hatanaka, *J. Synth. Org. Chem. Jpn.* **2001**, *59*, 996–1004.
- [63] Y. Hatanaka, *J. Organomet. Chem.* **2003**, *685*, 207–217.
- [64] K. Obata, C. Kabuto, M. Kira, *J. Am. Chem. Soc.* **1997**, *119*, 11345–11346.
- [65] H. S. Oh, L. S. Park, Y. Kawakami, *Chirality* **2003**, *15*, 646–653.
- [66] T. Sanji, K. Takase, H. Sakurai, *Bull. Chem. Soc. Jpn.* **2004**, *77*, 1607–1611.
- [67] M. Fujiki, *J. Am. Chem. Soc.* **1994**, *116*, 6017–6018.
- [68] M. Fujiki, *J. Organomet. Chem.* **2003**, *685*, 15–34.
- [69] H. Okumura, A. Kawaguchi, A. Harada, *Macromol. Rapid Commun.* **2002**, *23*, 781.
- [70] K. Sakamoto, T. Naruoka, M. Kira, *Chem. Lett.* **2003**, *32*, 380–381.
- [71] T. Sanji, A. Yoshiwara, H. Sakurai, M. Tanaka, *Chem. Commun.* **2003**, 1506–1507.
- [72] T. Sanji, M. Kato, M. Tanaka, *Macromolecules* **2005**, *38*, 4034–4037.
- [73] T. Sanji, N. Kato, M. Tanaka, *Chem. Lett.* **2005**, *34*, 1144–1145.
- [74] T. Sanji, N. Kato, M. Kato, A. Tanaka, *Angew. Chem. Int. Ed.* **2005**, *44*, 7301–7304; *Angew. Chem.* **2005**, *117*, 7467–7470.
- [75] H. Nakatsuji, *Chem. Phys. Lett.* **1978**, *59*, 362–364.
- [76] H. Nakatsuji, *Chem. Phys. Lett.* **1979**, *67*, 329–333.
- [77] C. Adamo, V. Barone, *J. Chem. Phys.* **1998**, *108*, 664–675.
- [78] E. C. Murray, R. N. Keller, *J. Org. Chem.* **1969**, *34*, 2234–2235.
- [79] M. Klessinger, J. Michl, *Excited States and Photochemistry of Organic Molecules*, Wiley-VCH, Weinheim, **1995**.
- [80] A. J. McCaffery, P. J. Stephens, P. N. Schatz, *Inorg. Chem.* **1967**, *6*, 1614–1625.
- [81] J. Michl, E. W. Thulstrup, *Spectroscopy with Polarized Light: Solute Alignment by Photoselection in Liquid Crystals, Polymers, and Membranes*, Wiley-VCH, Weinheim, **1995**.
- [82] A. D. Becke, *J. Chem. Phys.* **1993**, *98*, 5648–5652.
- [83] R. Krishnan, J. S. Binkley, R. Seeger, J. A. Pople, *J. Chem. Phys.* **1980**, *72*, 650–654.
- [84] C. Adamo, D. Jacquemin, *Chem. Soc. Rev.* **2013**, *42*, 845–856.
- [85] D. Jacquemin, E. A. Perpète, I. Ciofini, C. Adamo, R. Valero, Y. Zhao, D. G. Truhlar, *J. Chem. Theory Comput.* **2010**, *6*, 2071–2085.
- [86] D. Bousquet, R. Fukuda, P. Maitarad, D. Jacquemin, I. Ciofini, C. Adamo, M. Ehara, *J. Chem. Theory Comput.* **2013**, *9*, 2368–2379.
- [87] D. Bousquet, R. Fukuda, D. Jacquemin, I. Ciofini, C. Adamo, M. Ehara, *J. Chem. Theory Comput.* **2014**, *10*, 3969–3979.
- [88] H. Nakatsuji in *Computational Chemistry-Reviews of Current Trends, Vol. 2* (Ed.: J. Leszczynski), World Scientific, Singapore, **1997**, pp. 62–124.
- [89] M. Ehara, J. Hasegawa, H. Nakatsuji in *Theory and Applications of Computational Chemistry: The First 40 Years* (Eds.: C. E. Dykstra, G. Frenking, K. S. Kim, G. E. Scuseria), Elsevier, Oxford, **2005**.
- [90] H. Nakatsuji, *Chem. Phys.* **1983**, *75*, 425–441.
- [91] R. Fukuda, H. Nakatsuji, *J. Chem. Phys.* **2008**, *128*, 094105.
- [92] A. D. McLean, G. S. Chandler, *J. Chem. Phys.* **1980**, *72*, 5639–5648.
- [93] T. H. Dunning, Jr., P. J. Hay in *Methods of Electronic Structure Theory* (Ed.: H. F. Schaefer III), Plenum Press, New York, **1977**.
- [94] R. Fukuda, M. Ehara, *J. Comput. Chem.* **2014**, *35*, 2163–2176.
- [95] M. Ehara, R. Fukuda, C. Adamo, I. Ciofini, *J. Comput. Chem.* **2013**, *34*, 2498–2501.
- [96] C. Adamo, T. L. Bahers, M. Savarese, L. Wilbraham, G. García, R. Fukuda, M. Ehara, N. Rega, I. Ciofini, *Coord. Chem. Rev.* **2015**, *304–305*, 166–178.
- [97] Gaussian 09, Revision B.01, M. J. Frisch, G. W. Trucks, H. B. Schlegel, G. E. Scuseria, M. A. Robb, J. R. Cheeseman, G. Scalmani, V. Barone, B. Men-

nucci, G. A. Petersson, H. Nakatsuji, M. Caricato, X. Li, H. P. Hratchian, A. F. Izmaylov, J. Bloino, G. Zheng, J. L. Sonnenberg, M. Hada, M. Ehara, K. Toyota, R. Fukuda, J. Hasegawa, M. Ishida, T. Nakajima, Y. Honda, O. Kitao, H. Nakai, T. Vreven, J. A. Montgomery, Jr., J. E. Peralta, F. Ogliaro, M. Bearpark, J. J. Heyd, E. Brothers, K. N. Kudin, V. N. Staroverov, R. Kobayashi, J. Normand, K. Raghavachari, A. Rendell, J. C. Burant, S. S. Iyengar, J. Tomasi, M. Cossi, N. Rega, J. M. Millam, M. Klene, J. E. Knox, J. B., Cross, V. Bakken, C. Adamo, J. Jaramillo, R. Gomperts, R. E. Stratmann, O. Yazyev, A. J. Austin, R. Cammi, C. Pomelli, J. W. Ochterski, R. L. Martin, K. Morokuma, V. G. Zakrzewski, G. A. Voth, P. Salvador, J. J. Dannenberg,

S. Dapprich, A. D. Daniels, O. Farkas, J. B. Foresman, J. V. Ortiz, J. Cioslowski, D. J. Fox, Gaussian, Inc., Wallingford, CT, **2010**.
[98] F. Weinhold, J. E. Carpenter in *The Structure of Small Molecules and Ions* (Ed. R. Naaman, Z. Vager), Plenum, New York, **1988**, pp. 227–236.

Manuscript received: June 14, 2016
Accepted Article published: June 21, 2016
Final Article published: August 9, 2016